Comput Geosci (2017) 21:795–806
DOI 10.1007/s10596-017-9661-0

ORIGINAL PAPER

Adaptive dynamic/quasi-static pore network model for efficient multiphase flow simulation

Mohamed Regaieg[1] · **Arthur Moncorgé**[1]

Received: 16 January 2017 / Accepted: 3 May 2017 / Published online: 18 May 2017

Abstract Pore-scale simulation is increasingly used to study various phenomena that cannot be reproduced by conventional Darcy-based simulators. Direct numerical simulation on systems larger than a few millimeters is too computationally demanding. Pore network modeling (PNM) is a practical way to study the flow at pore scale for a representative elementary volume (REV) in a reasonable time. Pore network models can be divided into dynamic and quasi-static models. Dynamic models explicitly consider the competition between capillary and viscous forces. As they require pressure gradient calculation, they can be computationally expensive. Quasi-static models assume that the flow is only driven by capillary forces and avoids the need for pressure computations. Although they are very computationally efficient, the usage of these models is limited to capillary-dominated flow regimes obtained generally at low capillary numbers. We propose to combine the two approaches in an adaptive model, taking advantage of the speed of a quasi-static algorithm when the flow is governed by capillary forces, and that can simulate viscous effects when they are significant. We propose a criterion to localize the pressure solution in important areas to enhance the computational efficiency of the algorithm even in viscous dominated regimes. In this paper, we first describe our adaptive pore network model. Then, we show that using the capillary number as a switching criterion is not good enough to characterize the domain where the flow is controlled by capillary forces. Therefore, we present a newly defined criterion to switch between the dynamic and quasi-static flow regimes. Finally, we present several test cases where we show that the adaptive algorithm can considerably improve the computational performance of the pore network simulator without losing accuracy of the solution by treating large regions of models with the quasi-static algorithm. For capillary-dominated regimes, the observed speed-up can reach 16,000 for one million-node 3D networks. For viscous dominated regimes, the speed-up can reach 43 for one million-node 3D networks.

Keywords PNM · Pore scale · Speed-up · Dynamic · Quasi-static · Adaptive

1 Introduction

Flow in porous media is generally governed by the competition between viscous and capillary forces. However, the corresponding pore-scale phenomena determining the flow regime are not explicitly taken into account by classical reservoir simulators. As a consequence, reservoir simulators are unable to reproduce certain flow behaviours observed experimentally (Riaz et al. [16]). Pore network modelling (PNM) is a simulation technique that implements physics at the pore scale, and that can be used to understand the impact of parameters such as wettability, water salinity or pore size distribution on general flow behaviour. Pore network models of multiphase flow can be divided into dynamic and quasi-static models. Dynamic models explicitly consider the competition between capillary and viscous forces and therefore can simulate regimes such as viscous fingering and stable displacement. However, they can be computationally

✉ Mohamed Regaieg
mohamed.regaieg@total.com

Arthur Moncorgé
arthur.moncorge@total.com

[1] Geoscience Research Centre, Total E&P, Crawpeel Road, Altens, Aberdeen AB12 3FG, UK

expensive as they require computation of the pressure gradients. Dynamic models have been studied by several authors in recent decades. Some have used a single-pressure formulation where one pressure is assigned to a pore node regardless of its occupancy. In these models, either only a single fluid was present at the pore body/throat or both fluids could be present in the pore throat/body and an equivalent fluid can be defined with equivalent viscosity (Lenormand et al. [8]; McDougall and Sorbie [10]; Al-Gharbi [2]; Aghaei and Piri [1]; Regaieg [12]). A more recent approach of dynamic pore network models named two-pressure formulation considers each pore body filled with both fluids with each having each own pressure (Thompson [19]; Joekar-Niasar and Hassanizadeh [5]). Khayrat [6] used the pore network formulation of Joekar-Niasar and Hassanizadeh [5] and extended it by developing a multiscale hybrid approach in order to improve the computational efficiency of his dynamic pore network simulator. At low flow rates, the displacement tends to become dominated by capillary forces and simple flow rules can be defined to simulate the flow, thus avoiding pressure calculations (McDougall and Sorbie [11]; Valvatne and Blunt [20]; Ryazanov et al. [17]). These models are very efficient computationally; however, their usage is limited to capillary-dominated flow regimes obtained generally at low capillary numbers. The motivation for the current work is to overcome these shortcomings by combining the best of dynamic and quasi-static pore network models in a highly efficient adaptive pore network simulator which is based upon a single-pressure dynamic pore network model developed by Regaieg et al. [13] and Regaieg [12]. This model has been used in viscous fingering studies (Regaieg et al. [14]) and has been validated against micromodel experiments on a pore-by-pore basis and by comparing some macroscopic parameters such as saturation, relative permeability and saturation profiles (Yang et al. [21]).

We propose to develop an adaptive approach using a single-pressure dynamic pore network model which is faster than two-pressure simulators (Joekar-Niasar and Hassanizadeh [5]), but our approach and our criteria can also be applied to two-pressure pore network models. We do not use a multiscale algorithm as in Khayrat [6], but our method can be combined with a multiscale method for the global pressure computations. Firstly, we divide our pore network into coarse sub-networks that can be single phase, quasi static or dynamic. Single-phase sub-networks are kept unchanged as long as a two-phase interface is not entering in contact with them. For the quasi-static sub-networks, we do not need to compute the pressure and we can simulate the flow using a cheap quasi-static algorithm. However, in the dynamic sub-networks, we use a dynamic pore network model to simulate viscous effects and this requires calculating the pressure gradients in that sub-network. Secondly, we localize the pressure solution in the important areas only (i.e., at the interface between the fluids), making the code faster even in viscous dominated flow regimes. This makes the pressure matrices smaller. Finally, we need to perform global pressure solutions at a specified frequency to check if our choice of quasi-static and dynamic sub-networks is still valid. Subsequently, we adaptively modify the nature of the coarse sub-networks using a criterion based on the local physics. Although we do not yet use a multiscale approach to perform the global pressure solutions, we already observe very encouraging speed-ups in our algorithm compared to a fully dynamic code. In this paper, we first describe our adaptive pore network model. Then, we show that using the capillary number as a switching criterion is not reliable to characterize the domain where the flow is controlled by capillary forces. Therefore, we use a newly defined criterion to determine the capillary-dominated domains where it is relevant to use a quasi-static algorithm. Subsequently, we present test cases where the new adaptive algorithm considerably improves the computational performance of the pore network simulator without losing the accuracy of the solution. Finally, we report the speed-ups obtained with the adaptive algorithm for networks of several sizes on our implementation.

2 Description of the pore network model

2.1 Description of the dynamic algorithm

In this paper, we have used an improved version of the dynamic pore network model introduced by Regaieg et al. [12–15] to simulate fluid flow when viscous forces cannot be neglected. Firstly, a digital rock is either loaded from an extracted pore network (Dong and Blunt [4]) or generated stochastically from a given pore size distribution. The simulator offers the possibility to model the empty space in a rock either as an ensemble of pore bodies connected by throats or as a network of interconnected channels. We consider channel-only networks in all our simulations. However, the same work can be done using networks with more complex pore structure composed of pore bodies and pore throats. Once the network is loaded/created, all pore bodies and throats are filled with the defending phase (oil) and injection of the invading phase (water) begins. The network boundaries are considered closed, except for the inlet and outlet. We consider a constant injection rate boundary condition at the inlet where an injection channel is added before the network in order to make the pressure homogeneous at the inlet. However, at the outlet, we consider a fixed pressure boundary condition. The first step in simulating the

network flow consists of solving the pressure field which is the slowest step and generally accounts for about 90% of the simulation time.

Having solved the global pressure field, the local flow rates are computed from the pressure gradients and are used to update the fluid saturations at the pore throats/bodies situated across the interface between the fluids. We note that the interface between the phases is considered sharp and well defined and multiple pore throat and body invasions are possible; however, only one pore body/throat can be fully invaded during one time step. This feature makes possible the simulation of simultaneous menisci movements occurring at high rates (an important consideration when modelling viscous instabilities). We note that the incompressible nature of the fluids used in our simulations and the fact that the pressure equations are based on mass conservation ensure that we inject the appropriate volume of fluid at each time step. This procedure is then repeated until reaching a stopping condition which can either be attaining a fixed saturation value, reaching breakthrough, performing a fixed number of steps or injecting a fixed volume of the invading phase.

The two-phase flow within pore throats situated at the interface separating wetting and nonwetting phases must account for the capillary pressure drop across that interface. Using the Washburn formula

$$\begin{cases} Q_{ij} = G_{ij}\left(P_i - P_j + P_c\right), \text{if } P_i - P_j > -P_c \\ Q_{ij} = 0, \text{if} P_i - P_j \leq -P_c \end{cases} \quad (1)$$

where Q_{ij} is the dimensional flow rate from node i to j, G_{ij} is the dimensional conductance from nodes i to j, P_i is the pressure at node i and P_c is the capillary entry pressure defined by the Young-Laplace law

$$P_c = \frac{2\sigma \cos\theta}{R} \quad (2)$$

σ is the interfacial tension, θ is the contact angle ($\theta = 180°$ for a strongly oil wet system) and R is the radius of the pore throat. It should be noted that the capillary entry pressure is negative for an oil wet system. We note that the counter-flow invasions are not considered in this model but nothing prevents from including them in our adaptive approach.

The mass conservation equation for node 3 is written as (Fig. 1)

$$Q_{32} + Q_{34} + Q_{35} + Q_{36} = 0 \quad (3)$$

After writing the mass conservation for all the nodes of the network, we can write the problem in matrix form

$$G \times p = q_b + C_s \times q_c \quad (4)$$

where G is the matrix of conductances, p is the vector of pressures, q_b is the vector of source terms and q_c is the vector of capillary pressure effects. More details about the calculations can be found in Appendix.

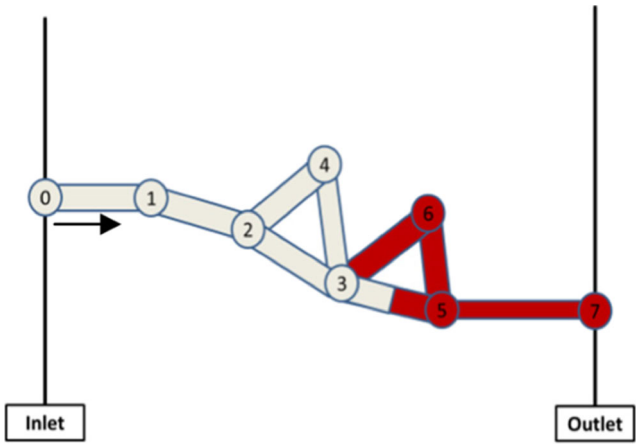

Fig. 1 A simple network of water injection (*white*) into oil (*red*)

2.2 Description of the adaptive algorithm

The first step consists in dividing the network into coarse sub-networks. This is followed by a global pressure solution. This allows us to find the state of each sub-network. There are three possible outcomes:

- Single-phase sub-network: If a single phase is present in this sub-network;
- Quasi-static sub-network: If two phases are present in this sub-network and the flow is dominated by capillary forces. The flow can be simulated using a quasi-static algorithm in this situation;
- Dynamic sub-network: If there are two phases in this sub-network and the viscous forces are affecting the flow. A dynamic algorithm is needed to simulate the flow in this sub-network.

For the moment, the grid is not optimized. For instance, we may have a situation where most of a sub-network is filled with a single phase and the sub-network may be considered dynamic. In the future, we may consider optimizing the grid by dividing such sub-networks into several smaller entities and thus having a smaller dynamic domain. The criterion determining if the sub-network is dynamic or quasi static is discussed in detail in the next section of this paper.

After identifying the state of the sub-networks, we compute the localized pressure matrix using only the dynamic sub-networks and considering the pressures from the global solution as boundary conditions of our localized problem. For instance, in the example of Figs. 2 and 3, the conductance matrix size will be 8×8 instead of 36×36 which improves the computational performance. Subsequently, we

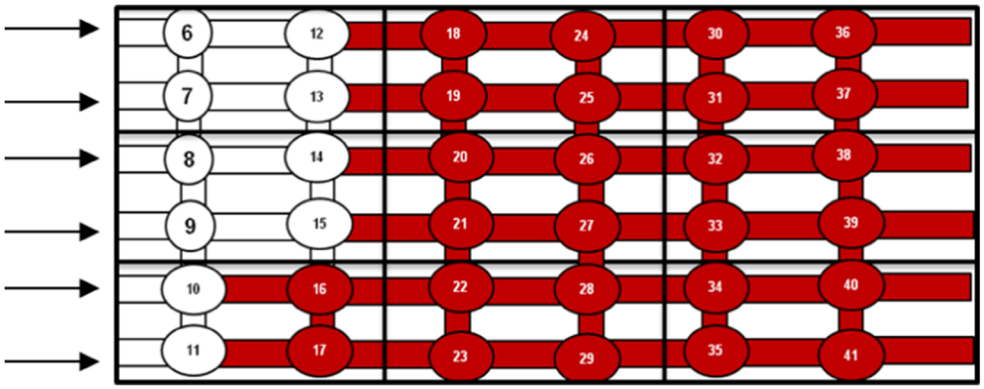

Fig. 2 A schematic figure showing a pore network where water (white) is injected into oil (*red*). The black lines show the limits of each sub-network

adaptively modify the nature of the coarse sub-networks using a criterion based on the local physics. In order to determine the new state of the sub-networks, a global pressure solution is needed after few time steps and the frequency of the global pressure solution is chosen by the user. Moreover, we make sure that the mass is conserved for every quasi-static and dynamic sub-network. This is done by computing the volume entering the quasi-static sub-networks and updating their saturation using a quasi-static algorithm.

The algorithm can be summarized as follows:

1. The pore network is divided into sub-networks;
2. The pressure is solved globally;
3. The pressure is solved for the dynamic domain, and the saturation is updated accordingly until reaching the global pressure solution frequency;
4. The volumes entering the quasi-static sub-networks are recorded, and the saturations are updated in order to keep the mass conservation;
5. This is repeated.

3 Switching criterion

The interplay of the viscous and capillary forces completely determines the flow regime. For instance, if the displacement is dominated by capillary forces, capillary fingering regime is obtained, whilst if the flow is dominated by viscous forces, a stable displacement flow is obtained for favourable viscosity ratios and viscous fingering regime is observed for unfavourable viscosity ratios. Finding the correct domain of capillary fingering regime where capillary forces dominate the flow is crucial for our model in order to maximize the usage of the quasi-static algorithm without losing the accuracy of the solution. Usually, the capillary number is used to define the limits of the capillary fingering regime. The capillary number is a measure of the viscous to capillary forces balance and is usually defined as (Lake [7])

$$Nca = \frac{\mu_{\text{invading}}\mathbf{V}}{\sigma} \tag{5}$$

where μ_{invading} is the viscosity of the invading fluid, $\mathbf{V}$ is the Darcy velocity and σ is the interfacial tension between the invading and defending fluids.

However, the classical definition of the capillary number has several limits because the physical justification for defining the capillary number is often absent (Cense and Berg [3]). This classic definition does not take into account other parameters such as the contact angle value and the viscosity ratio which have important effects on the force balance between viscous and capillary forces. Moreover, it

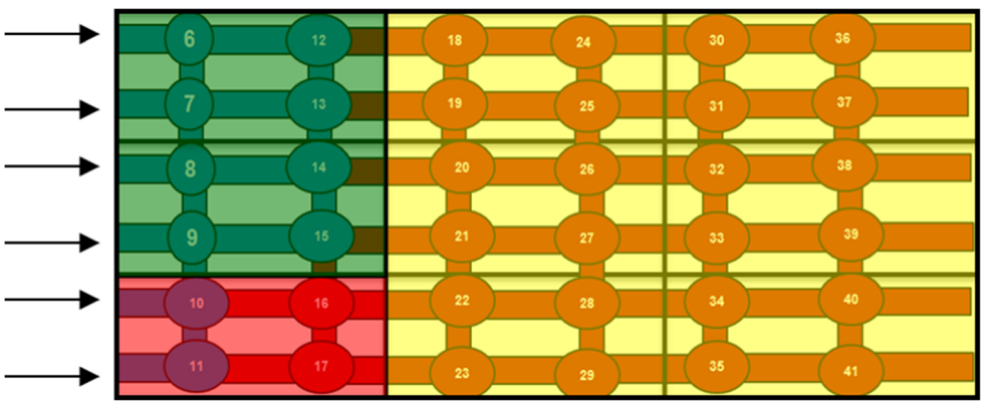

Fig. 3 A schematic figure showing a pore network with sub-networks having different states. The *green colour* shows the dynamic sub-networks, the *red colour* shows the quasi-static sub-networks and the *yellow colour* shows the single-phase sub-networks

is generally considered that capillary numbers of the order of $\mathbf{10^{-6}}$ correspond to capillary-dominated behaviour (Lake [7]). However, Skauge et al. [18] have performed water-flooding experiments in heavy oil where they observed a viscous fingering phenomenon for capillary numbers of the order of $\mathbf{10^{-9}}$. Lenormand et al. [8] have proposed that immiscible displacements in porous media with both capillary and viscous effects can be characterized by two dimensionless numbers; the capillary number, which is the ratio of viscous forces to capillary forces; and the viscosity ratio of the fluids. For certain values of these numbers, either viscous or capillary forces dominate and determine the flow regime. However, Zhang et al. [22] have performed a similar study using different micromodels and created a phase diagram delimiting the domain of each flow regime. The boundaries of their phase diagram were different from the ones obtained by Lenormand et al. [8]. Combining the capillary number with the viscosity ratio information may not even be enough to determine the balance of viscous and capillary forces. Therefore, using a threshold capillary number to choose whether viscous forces are important for the flow is not practical as for each set of parameters (viscosity ratio, wettability, etc.), the threshold capillary number is different. In a recent work, Regaieg and Moncorge [15] have considered the macroscopic capillary number to determine the capillary fingering domain. This criterion was efficient for drainage simulations. But, it required a "magic" threshold number to be chosen and was difficult to generalize to more complicated wettability scenarios. When a global pressure solution is performed, the pore bodies and pore throats that are accessible to the invading phase are determined. If these pores follow the filling order that a quasi-static algorithm would predict in a particular sub-network, we assume that this sub-network is quasi static. Otherwise, if the global pressure solution shows that the pore throats and bodies accessible dynamically in a sub-network are different from what a quasi-static algorithm would predict, we consider that the viscous forces are affecting the flow and we consider that the sub-network is dynamic. For instance, after a global pressure solution, the saturation is updated and menisci advance in some pore throats/nodes. In the drainage situation illustrated in Fig. 4a, the largest pore throat was invaded dynamically. This follows the invasion order of a quasi-static algorithm. This is a clear indication that the flow is capillary dominated. Therefore, if such situation occurs in a sub-network, it is considered quasi static. However, if following a global pressure solution, a situation similar to Fig. 4b, c is observed where the filling order is different from the quasi-static order—in these particular examples, small pore throats were filled before larger ones in a drainage scenario, the viscous forces are affecting the flow and the sub-network is considered dynamic.

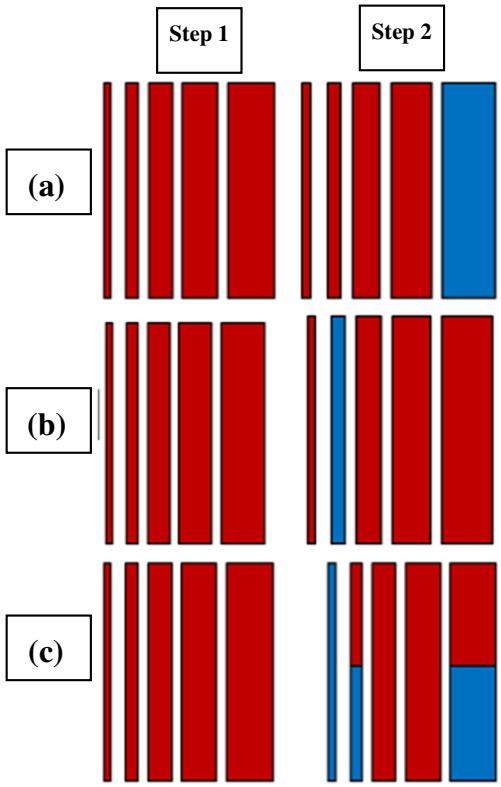

Fig. 4 Filling for a drainage scenario in three different situations after a global pressure solution. **a** Viscous forces do not affect the flow. **b** Viscous forces affect the flow and change the order of the filling sequence. **c** Viscous forces affect the flow, and multiple-pore filling is observed into pore throats with different sizes

This criterion is general and automatic and does not need magic threshold numbers to decide whether the viscous forces are affecting the flow.

4 Simulations

We propose to test our adaptive pore network algorithm using several viscosity ratios, injection rates and wettability scenarios to study the accuracy and the robustness of our switching criterion. We consider relatively small unstructured networks (200×200), and we compare the saturation maps for the adaptive and the fully dynamic model. All these simulations were performed using constant rate injection boundary conditions, 8×8 mesh and a global pressure frequency of 50 – the global pressure is resolved after 50 invasions. Figures 5, 6, 7, 8, 9 and 10 show that for all the cases, despite small minor differences, the adaptive algorithm could reproduce similar saturation maps to the ones obtained with the fully dynamic pore network simulator. These simulations cover a wide range of viscosity ratios, injection rates and wettability scenarios, giving us

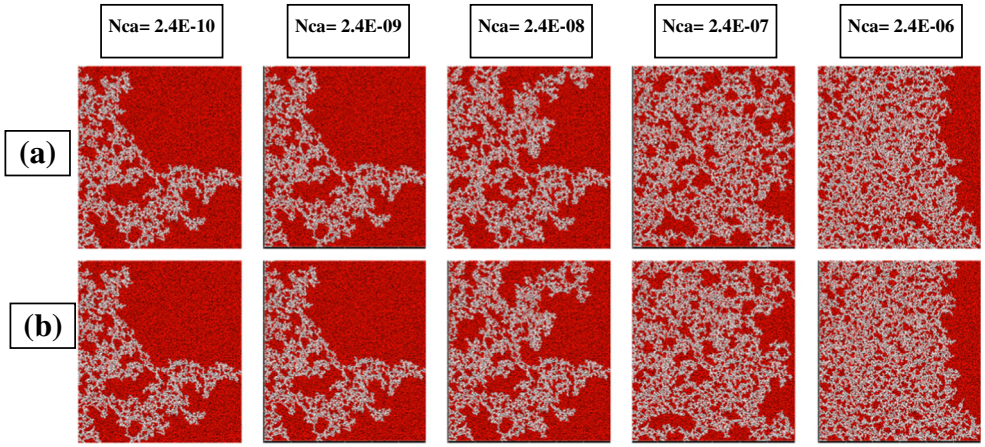

Fig. 5 Comparison between the saturation maps of fully dynamic (**a**) and adaptive (**b**) constant rate injection simulations for several capillary numbers, a viscosity ratio $M = 1$ and strongly oil wet conditions

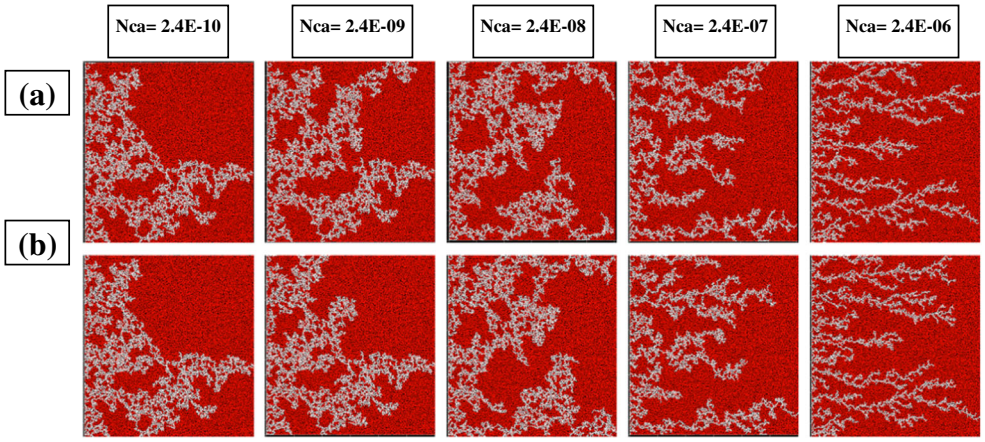

Fig. 6 Comparison between the saturation maps of fully dynamic (**a**) and adaptive (**b**) constant rate injection simulations for several capillary numbers, a viscosity ratio $M = 100$ and strongly oil wet conditions

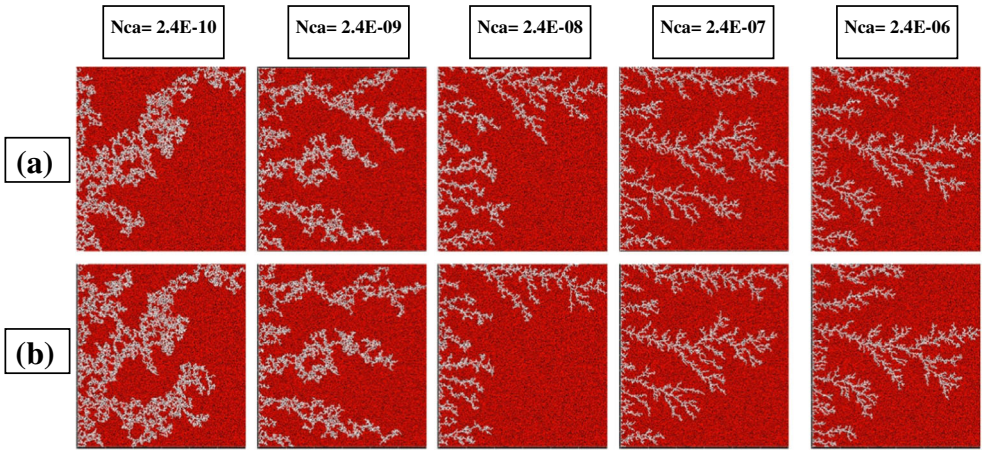

Fig. 7 Comparison between the saturation maps of fully dynamic (**a**) and adaptive (**b**) constant rate injection simulations for several capillary numbers, a viscosity ratio $M = 7000$ and strongly oil wet conditions

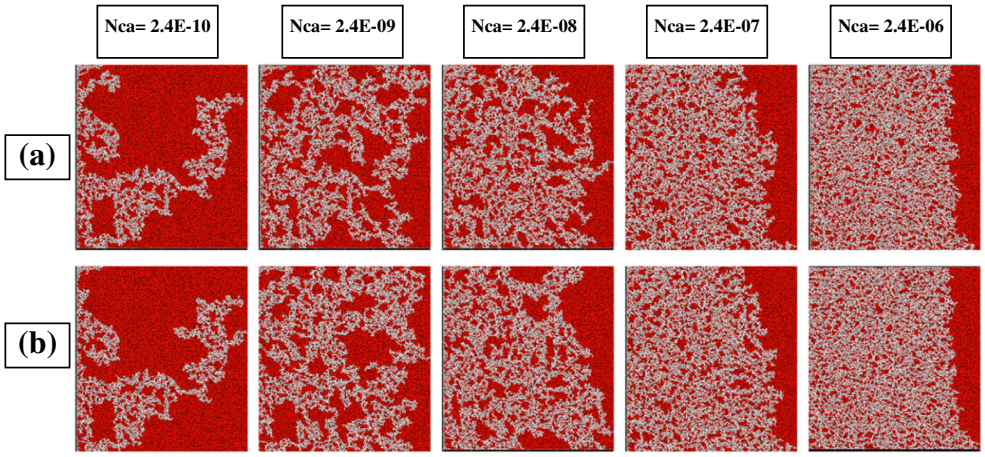

Fig. 8 Comparison between the saturation maps of fully dynamic (**a**) and adaptive (.) constant rate injection simulations for several capillary numbers, a viscosity ratio $M = 1$ and strongly water wet conditions

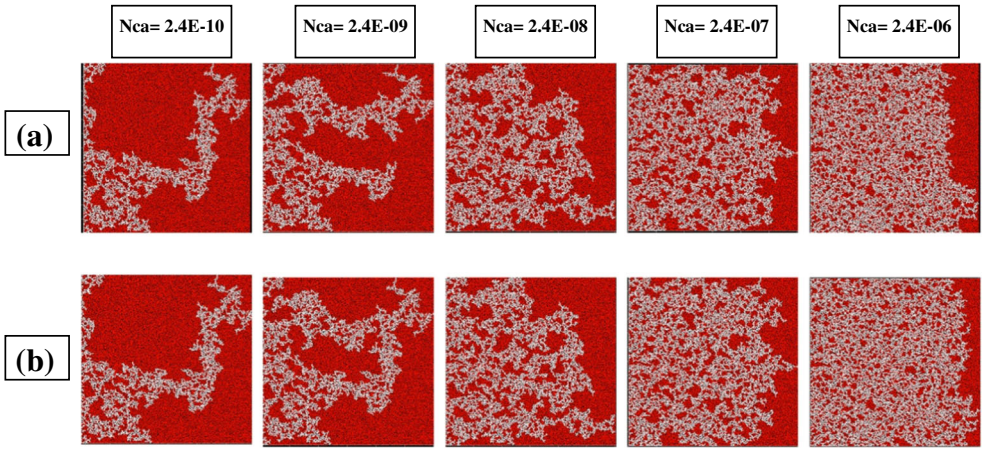

Fig. 9 Comparison between the saturation maps of fully dynamic (**a**) and adaptive (**b**) constant rate injection simulations for several capillary numbers, a viscosity ratio $M = 1$ and fractional wet conditions

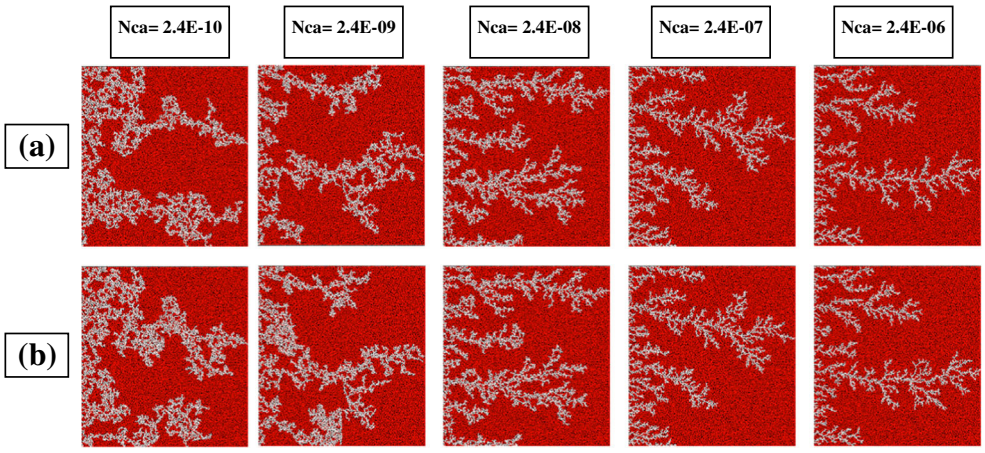

Fig. 10 Comparison between the saturation maps of fully dynamic (**a**) and adaptive (**b**) constant rate injection simulations for several capillary numbers, a viscosity ratio $M = 7000$ and strongly water wet conditions

confidence in our switching criterion. We note that at low rates, the simulations are 100% quasi static. However, as the rate increases, more dynamic regions are considered. This is demonstrated in Fig. 11 where we observe the cumulative dynamic sub-network percentage in the simulations of Figs. 5b, 6b and 7b. These plots show the dynamic domain evolution as a function of saturation. At high injection rates and an unfavourable viscosity ratio, a viscous fingering regime is observed and large areas of the network are not swept as a result of the viscous instability. These areas can be considered as single-phase sub-networks and are removed from the pressure matrices result in faster simulations. This can be confirmed by Fig. 11 that the dynamic percentage in this regime never exceeded 40% in the considered cases. At high injection rates and a favourable viscosity ratio, although the sweep efficiency was good, the adaptive algorithm was very efficient and the dynamic percentage was lower than 20% (Fig. 11). Actually, mainly the sub-networks at the saturation front were dynamic in this regime and the sub-networks behind the front were quasi-static. This shows that, for all the flow regimes, the adaptive algorithm was very efficient and the dynamic domain was

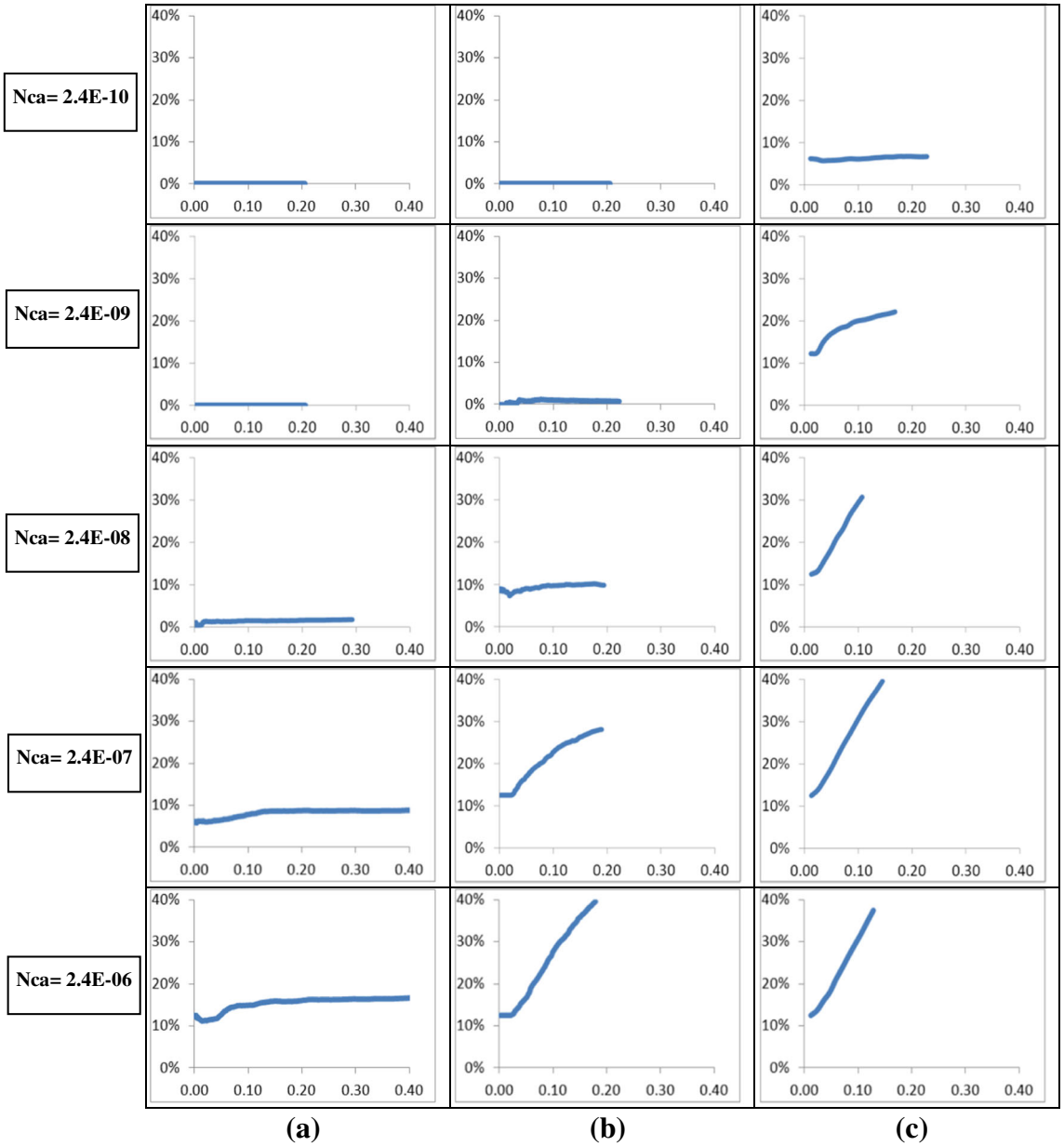

Fig. 11 Comparison between the cumulative dynamic sub-network percentage in the constant rate injection simulations of Figs. 7b, 8b and 9b. These *curves* show the dynamic domain evolution as a function of invading phase saturation for viscosity ratios $M = 1$ (**a**), $M = 100$ (**b**) and $M = 7000$ (**c**) and for several capillary numbers

smaller than 40% of the network in all the cases. We note here that the dynamic domain can become smaller by optimizing the grid meshing, an exercise that was not done in these simulations. We point out that our algorithm does not take into account the interaction between the dynamic and the non-dynamic domains between global pressure solutions. For all the considered cases, this assumption proved to be reasonable. However, if more challenging situations are encountered, this may not be the case anymore. A possible way to solve this is to increase the global pressure frequency which leads to a better agreement with the dynamic simulations as shown in Fig. 12. For the moment, finding the appropriate global frequency is not automatic. However, we are currently working on implementing an automatic criterion to detect if global pressure solutions are needed. Although we only presented test cases with constant rate boundary, we have verified that our algorithm can also be used on constant pressure simulations.

The simulations performed on small networks showed that the adaptive algorithm gives better computational performance than the fully dynamic pore network model whilst keeping a good accuracy. Still, the real potential of the algorithm can be mainly realized for simulations performed on larger networks. Therefore, we perform a series of simulations for different network sizes in order to quantify the speed-ups realized using the adaptive algorithm. Whilst the speed-ups that we observe are obviously dependent on the implementation, they provide an idea about the potential of the approach. The numerical parameters used in these simulations are reported in Table 1. First, we consider a capillary fingering case where the enhancement of the computational performance is realized by avoiding solving the pressure and using a quasi-static algorithm. As we can see in Fig. 13, better computational performance was achieved. For instance, for

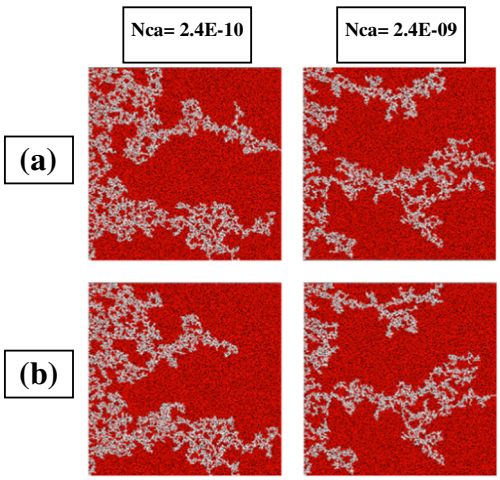

Fig. 12 Comparison between the saturation maps of fully dynamic (**a**) and adaptive (**b**) simulations of Fig. 10 with higher global pressure frequencies of 10 ($Nca = 2.4E-10$) and 25 ($Nca = 2.4E-09$)

Table 1 Numerical parameters of the simulations of Figs. 11, 12, 13, 14, 15 and 16

Network size	Mesh	Global frequency
200 × 200	10 × 10	100
500 × 500	25 × 25	250
1000 × 1000	50 × 50	500
35 × 35 × 35	3 × 3 × 3	100
50 × 50 × 50	5 × 5 × 5	250
100 × 100 × 100	10 × 10 × 10	500

a 43,000-node 3D pore network, the adaptive algorithm was 560 times faster, and for one million-node 3D network, the adaptive algorithm was 16,000 times faster than the fully dynamic algorithm. We also notice that the speed improvement was greater in 3D networks, which was expected as solving the pressure in 3D topology is more complex than that in 2D. Subsequently, we consider a viscous fingering regime where large areas are left unswept and thus can be considered as single phase. Therefore, large parts of the network can be removed from the pressure calculations. Although these simulations were viscous dominated, better computational efficiency was achieved using the adaptive algorithm. We observed in 2D simulations a speed-up of 4 for a 43,000-node 2D network and 15 for a one million-node network (Fig. 14). Three-dimensional simulations of viscous fingering regime showed speed-ups of 5.0 for a 43,000-node network and 30 for a one million-node network. Finally, we consider a stable displacement regime where the dynamic calculations were mainly performed at the saturation front and avoided in the already swept and single-phase areas. Therefore, the pressure matrices become smaller and speed-ups are observed. For 2D simulations, a speed-up of 4.5 for a 43,000-node 2D network and 17 for a one million-node network (Fig. 15). Three-dimensional simulations of stable displacement regime showed speed-ups of 6.0 for a 43,000-node network and 43 for a one million-node network. We note that our code does not consider the ganglia mobilization phenomenon for the moment. This means that if we would like to simulate such phenomenon, more dynamic regions should be considered even behind the waterfront.

As these running times may depend on the specificities of the implementation, in addition to reporting the speed-ups of Figs. 13, 14 and 15, we also report the percentage of dynamic sub-networks during the simulations in Figs. 16, 17 and 18. For all the cases, the dynamic domain is less than 40% of the total domain. Moreover, it is observed that the larger the network, the smaller the dynamic domains. Most dynamic regions are situated at the injection front, and these regions represent a smaller fraction of the total system for larger and larger networks. As a consequence, the larger the network, the more efficient is the adaptive algorithm.

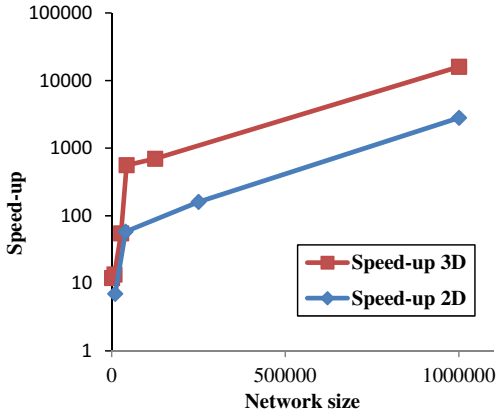

Fig. 13 Speed-up of the adaptive algorithm compared to the fully dynamic one for capillary-dominated constant rate injection simulations performed at different network sizes with a viscosity ratio $M = 1$. In these simulations, 2D and 3D networks were used and the running times were compared at invading phase saturation of 5%

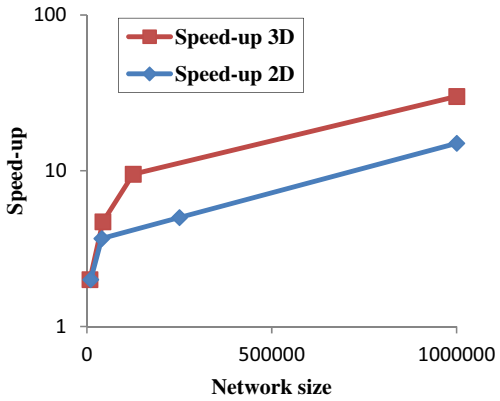

Fig. 14 Speed-up of the adaptive algorithm compared to the fully dynamic one for viscous fingering constant rate injection simulations performed at different network sizes with a viscosity ratio $M = 7000$. In these simulations, 2D and 3D networks were used and the running times were compared at invading phase saturation of 5%

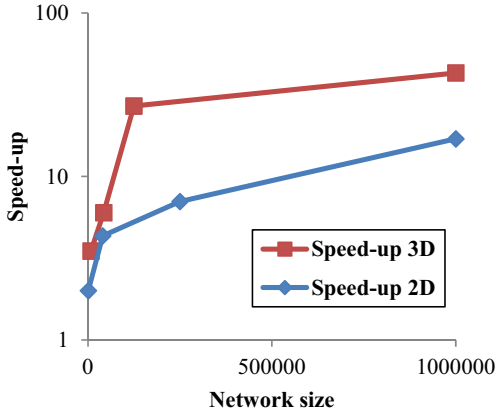

Fig. 15 Speed-up of the adaptive algorithm compared to the fully dynamic one for stable displacement regime performed at different network sizes with a viscosity ratio $M = 1$. In these constant rate injection simulations, 2D and 3D networks were used and the running times were compared at invading phase saturation of 5%

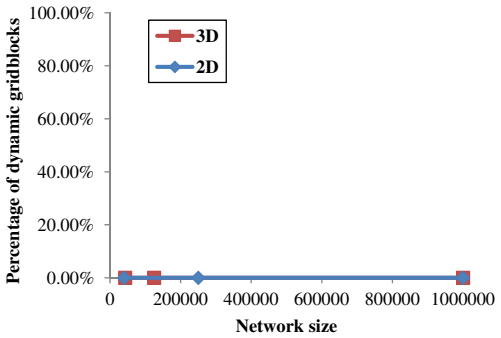

Fig. 16 Percentage of dynamic sub-networks for capillary-dominated simulations performed at different network sizes with a viscosity ratio $M = 1$. In these simulations, 2D and 3D networks were used and the running times were compared at invading phase saturation of 5%. As the test cases are 100% quasi static, the percentage of dynamic sub-networks stays at 0%

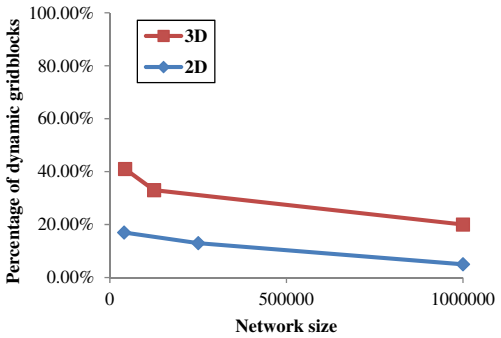

Fig. 17 Percentage of dynamic sub-networks for viscous fingering simulations performed at different network sizes with a viscosity ratio $M = 7000$. In these simulations, 2D and 3D networks were used and the running times were compared at invading phase saturation of 5%

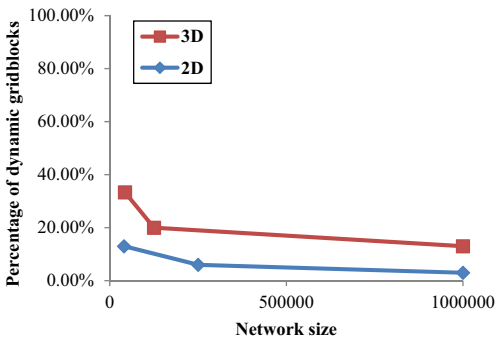

Fig. 18 Percentage of dynamic sub-networks for stable displacement simulations performed at different network sizes with a viscosity ratio $M = 1$. In these simulations, 2D and 3D networks were used and the running times were compared at invading phase saturation of 5%

5 Conclusions

In this paper, an adaptive pore network model has been developed and applied to a range of simulations with different viscosity ratios and wettability scenarios. We combine quasi-static and dynamic pore network models in an adaptive algorithm that takes advantage of the speed of quasi-static algorithms when flow is governed by capillary forces, and that can simulate the viscous effects when they are important. The network was divided into several sub-networks, and the state of the force balance in each sub-network was determined using a newly defined criterion. Furthermore, for viscous dominated simulations, this algorithm localizes the pressure solution within the invaded zone, thus removing single-phase regions from the pressure matrix. This has resulted in improvements of the computational efficiency of our code for all the flow regimes. This algorithm can be used for single-pressure and two-pressure algorithms and can also be combined with a multiscale approach to solve the global pressure systems. This work made possible the simulation of large systems of tens of centimeters. In Loubens et al. [9], we have simulated viscous fingering in 2D systems as large as 3×90 cm and compared them to X-ray images of the corresponding experiments.

Acknowledgments The authors would like to thank the TOTAL management for the authorization to publish this work.

Appendix

In the example of Fig. 1, after writing the dimensional mass conservation equation for node 3 (contributions from nodes 2, 4, 5 and 6), we have

$$G_{32}\,(P_3 - P_2) + G_{34}\,(P_3 - P_4) + G_{35}\left(P_3 - P_5 + \frac{2\sigma\cos\theta_{35}}{R_{35}}\right) + G_{36}\left(P_3 - P_6 + \frac{2\sigma\cos\theta_{36}}{R_{36}}\right) = 0 \quad (6)$$

where

- P_s is the pressure scale;
- L_s is the length scale;
- G_s is the conductance scale taken as $G_s = \frac{L_S^3}{P_s T_s}$ (where T_s is a time scale always taken equal to 1);
- R_{ij} is the radius of the throat relating nodes i and j.

After dividing (1) by $G_s P_s$, we obtain the non-dimensional form:

$$(g_{32} + g_{34} + g_{35} + g_{36})p_3 - g_{32}p_2 - g_{34}p_4 - g_{35}p_5 - g_{36}p_6 = C_s g_{35}\left(-\frac{\cos\theta_{35}}{r_{35}}\right) + C_s g_{36}\left(-\frac{\cos\theta_{36}}{r_{36}}\right) \quad (7)$$

where g_{ij} is the non-dimensional conductance between nodes i and j, p_i is the non-dimensional pressure of node i, C_s is the capillary scale defined as $C_s = \frac{2\sigma}{P_s L_s}$ and r_{ij} is the non-dimensional radius of the throat between nodes i and j.

Note that the RHS of Eq. 2 includes a term representing the effect of the capillary entry pressure, making the matrix form of the problem as $G \times p = q_b + C_s \times q_c$. For the example of Fig. 1, the pressure matrix and vectors become

$$G = \begin{pmatrix} g_1 & -g_{12} & 0 & 0 & 0 & 0 \\ -g_{12} & g_2 & -g_{23} & -g_{24} & 0 & 0 \\ 0 & -g_{23} & g_3 & -g_{34} & -g_{35} & -g_{36} \\ 0 & -g_{24} & -g_{34} & g_4 & 0 & 0 \\ 0 & 0 & -g_{35} & 0 & g_5 & -g_{56} \\ 0 & 0 & -g_{36} & 0 & -g_{56} & g_6 \end{pmatrix}, p = \begin{pmatrix} p_1 \\ p_2 \\ p_3 \\ p_4 \\ p_5 \\ p_6 \end{pmatrix}, q_b = \begin{pmatrix} q_{01} \\ 0 \\ 0 \\ 0 \\ 0 \\ 0 \end{pmatrix}, \text{and}$$

$$q_c = \begin{pmatrix} 0 \\ 0 \\ g_{35} \times \left(-\frac{\cos\theta 35}{r35}\right) + g_{36} \times \left(-\frac{\cos\theta 36}{r36}\right) \\ 0 \\ g_{35} \times \left(\frac{cos\theta 35}{r35}\right) \\ g_{36} \times \left(\frac{cos\theta 36}{r36}\right) \end{pmatrix}$$

where we have defined

$$\begin{pmatrix} g_1 \\ g_2 \\ g_3 \\ g_4 \\ g_5 \\ g_6 \end{pmatrix} = \begin{pmatrix} g_{12} \\ g_{12} + g_{23} + g_{24} \\ g_{23} + g_{34} + g_{35} + g_{36} \\ g_{24} + g_{34} \\ g_{35} + g_{56} + g_{57} \\ g_{56} + g_{36} \end{pmatrix}$$

and

- q_b and q_c are respectively the vector of source terms and the vector of capillary effects at fluid-fluid interfaces.
- q_{01} represents the fixed injection rate at the inlet (between nodes 0 and 1).

References

1. Aghaei, A., Piri, M.: Direct pore-to-core up-scaling of displacement processes: dynamic pore network modeling and experimentation. J. Hydrol. **522**, 488–509 (2015)
2. Al-Gharbi, M.S.: Dynamic pore-scale modelling of two-phase flow. Imperial College (2004)
3. Cense, A., Berg, S.: The viscous-capillary paradox in 2-phase flow in porous media. In: International Symposium of the Society of Core Analysts held in Noordwijk, The Netherlands, pp. 27–30 (2009)

4. Dong, H., Blunt, M.J.: Pore-network extraction from micro-computerized-tomography images. Phys. Rev. E **80**(3), 036307 (2009)
5. Joekar-Niasar, V., Hassanizadeh, S.M.: Uniqueness of specific interfacial area–capillary pressure–saturation relationship under non-equilibrium conditions in two-phase porous media flow. Transp. Porous Media **94**(2), 465–486 (2012). 10.1007/s11242-012-9958-3
6. Khayrat, K.: Modeling hysteresis for two-phase flow in porous media: from micro to macro scale. Dissertation, ETH-Zürich, 2016, Nr. 23273 (2016)
7. Lake, L.W.: Enhanced oil recovery (1989)
8. Lenormand, R., Touboul, E., Zarcone, C.: Numerical models and experiments on immiscible displacements in porous media. J. Fluid Mech. **189**, 165–187 (1988)
9. Loubens, R.D., Vaillant, G., Regaieg, M., Yang, J., Moncorgé, A., Fabbri, C., Darche, G.: Numerical modeling of unstable water floods and tertiary polymer floods into highly viscous oils. In: SPE Reservoir Simulation Conference, Society of Petroleum Engineers (2017)
10. McDougall, S., Sorbie, K.: The combined effect of capillary and viscous forces on waterflood displacement efficiency in finely laminated porous media. In: SPE Annual Technical Conference and Exhibition, Society of Petroleum Engineers (1993)
11. McDougall, S.R., Sorbie, K.: The impact of wettability on waterflooding: pore-scale simulation. doi:10.2118/25271-PA (1995)
12. Regaieg, M.: Pore network modelling of fingering phenomena during unsteady-state waterflooding of heavy oils. Heriot-Watt University (2015)
13. Regaieg, M., McDougall, S., Bondino, I., Hamon, G.: Finger thickening during extra-heavy oil waterflooding: simulation and interpretation using pore-scale modelling (2014)
14. Regaieg, M., McDougall, S., Bondino, I., Hamon, G.: Finger thickening during extra-heavy oil waterflooding: simulation and interpretation using pore-scale modelling. PLOS ONE (2017)
15. Regaieg, M., Moncorge, A.: Improving the computational efficiency of a dynamic pore network model—a hybrid approach for a better performance. In: ECMOR XIV-15th European Conference on the Mathematics of Oil Recovery (2016)
16. Riaz, A., Tang, G.-Q., Tchelepi, H.A., Kovscek, A.R.: Forced imbibition in natural porous media: comparison between experiments and continuum models. Phys. Rev. E **75**(3), 036305 (2007)
17. Ryazanov, A.V., Van Dijke, M.I.J., Sorbie, K.S.: Two-phase pore-network modelling: existence of oil layers during water invasion. Transp. Porous Media **80**(1), 79–99 (2009). doi:10.1007/s11242-009-9345-x
18. Skauge, A., Ormehaug, P.A., Gurholt, T., Vik, B., Bondino, I., Hamon, G.: 2-D visualisation of unstable waterflood and polymer flood for displacement of heavy oil. In: SPE Improved Oil Recovery Symposium, Society of Petroleum Engineers (2012)
19. Thompson, K.E.: Pore-scale modeling of fluid transport in disordered fibrous materials. AIChE J. **48**(7), 1369–1389 (2002)
20. Valvatne, P.H., Blunt, M.J.: Predictive pore-scale modeling of two-phase flow in mixed wet media. Water Resour. Res. **40**, 7 (2004)
21. Yang, J., Bondino, I., Regaieg, M., Moncorgé, A.: Pore to pore validation of pore network modelling against micromodel experiment results. Computational Geosciences, pp. 1–14. doi:10.1007/s10596-017-9630-7 (2017)
22. Zhang, C., Oostrom, M., Wietsma, T.W., Grate, J.W., Warner, M.G.: Influence of viscous and capillary forces on immiscible fluid displacement: pore-scale experimental study in a water-wet micromodel demonstrating viscous and capillary fingering. Energy Fuels **25**(8), 3493–3505 (2011). doi:10.1021/ef101732k